Published in final edited form as:
Biochemistry. 2014 January 14; 53(1): 202–213. doi:10.1021/bi401022b.

A Noncompetitive Inhibitor for *Mycobacterium tuberculosis's* Class IIa Fructose 1,6-Bisphosphate Aldolase

Glenn C. Capodagli[†], **Wafik G. Sedhom**[†], **Mary Jackson**[‡], **Kateri A. Ahrendt**[*,§], and **Scott D. Pegan**[*,†,∥]

[†]Department of Chemistry and Biochemistry, University of Denver, Denver, Colorado 80208, United States

[‡]Mycobacteria Research Laboratories, Department of Microbiology, Immunology and Pathology, Colorado State University, Fort Collins, Colorado 80523, United States

[§]Department of Chemistry, Regis University, Denver, Colorado 80221, United States

[∥]Eleanor Roosevelt Institute, University of Denver, Denver, Colorado 80208, United States

Abstract

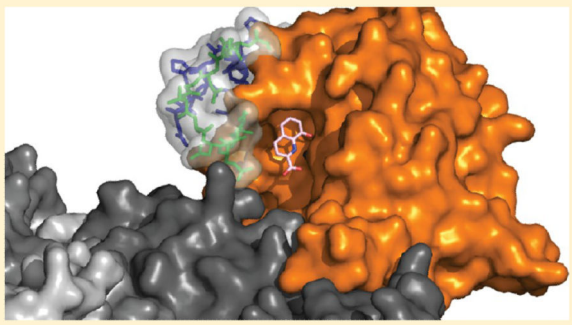

Class II fructose 1,6-bisphosphate aldolase (FBA) is an enzyme critical for bacterial, fungal, and protozoan glycolysis/gluconeogenesis. Importantly, humans lack this type of aldolase, having instead a class I FBA that is structurally and mechanistically distinct from class II FBAs. As such, class II FBA is considered a putative pharmacological target for the development of novel antibiotics against pathogenic bacteria such as *Mycobacterium tuberculosis*, the causative agent for tuberculosis (TB). To date, several competitive class II FBA substrate mimic-styled inhibitors have been developed; however, they lack either specificity, potency, or properties that limit their potential as possible therapeutics. Recently, through the use of enzymatic and structure-based assisted screening, we identified 8-hydroxyquinoline carboxylic acid (HCA) that has an IC_{50} of 10

[*]**Corresponding Authors** Department of Chemistry, Regis University, 3333 Regis Blvd., Denver, CO 80221. kahrendt@regis.edu. Telephone: (303) 964-5088. Eleanor Roosevelt Institute and Department of Chemistry and Biochemistry, University of Denver, 2190 E. Iliff Ave., Olin 202, Denver, CO 80208. spegan@du.edu. Telephone: (303) 871-2533..

Supporting Information Omit maps and *B* factors of atoms near HCA (Figure S1). This material is available free of charge via the Internet at http://pubs.acs.org.

Accession Codes The atomic coordinates and structure factors have been deposited as Protein Data Bank entry 4LV4.

The authors declare the following competing financial interest(s): A provisional U.S. Patent Application, 61/821,184, has been filed.

± 1 μM for the class II FBA present in *M. tuberculosis* (MtFBA). As opposed to previous inhibitors, HCA behaves in a noncompetitive manner, shows no inhibitory properties toward human and rabbit class I FBAs, and possesses anti-TB properties. Furthermore, we were able to determine the crystal structure of HCA bound to MtFBA to 2.1 Å. HCA also demonstrates inhibitory effects for other class II FBAs, including pathogenic bacteria such as methicillin-resistant *Staphylococcus aureus*. With its broad-spectrum potential, unique inhibitory characteristics, and flexibility of functionalization, the HCA scaffold likely represents an important advancement in the development of class II FBA inhibitors that can serve as viable preclinical candidates.

Tuberculosis (TB) is one of the most prevalent infections in the world and a leading cause of mortality in developing countries.[1] *Mycobacterium tuberculosis*, the causative agent for TB infections, have been estimated by the World Health Organization (WHO) at 8.7 million new cases during 2011, with 1.4 million *M. tuberculosis-related* deaths.[2] This brings the total number of estimated new cases and deaths over the past five years to a staggering 45.6 million and 8.1 million, respectively. Additionally, one-third of the world's population is estimated to have latent *M. tuberculosis*.[1] Further exacerbating the danger of TB is the considerable rise of TB co-infecting patients with HIV. Specifically, individuals infected with HIV are more than 20 times more likely to develop active TB and thus be able to rapidly spread the disease.[2,3] The current treatment for TB, Directly Observed Therapy, Short Course (DOTS), relies on directly observing the administration of a four-drug cocktail over a two month span with continuous two-drug treatments for an additional two–four months.[4]

In recent years, the WHO has estimated that the rate of curing TB with DOTS has declined from 95 to 85%.[2] A significant factor in this decline, which has thwarted intensifying efforts to eliminate TB, is increasing drug resistance. Incidences of multidrug-resistant TB (MDR-TB), TB resistant to the two most efficacious TB drugs, are on the rise, with 500,000 cases reported in 2011.[2] Also, spreading of extensively drug-resistant TB (XDR-TB), MDR-TB with additional resistance to almost all known TB drugs, has occurred. As of 2011, XDR-TB has appeared in 84 countries, including the United States.[2] For MDR-TB, new treatment regimens, including DOTS plus, have been initiated but require 18 months of treatment.[5] Treatment options for XDR-TB are even more limited.[5] Also, the practicality of these prolonged pharmacological treatments is largely in doubt, as patient compliance difficulties have already been encountered during the six month DOTS treatment.[5]

The absence of an effective treatment for MDR-TB and XDR-TB and the increase in the number of active TB cases among HIV patients highlight the need to explore other potential TB drug targets. One widely touted potential drug target is *M. tuberculosis's* sole fructose 1,6-bisphosphate aldolase (MtFBA, EC 4.1.2.13).[6–17] As a class II fructose 1,6-bisphosphate aldolase, MtFBA falls into one of two classes of fructose 1,6-bisphosphate aldolases (FBAs). Both class I and class II FBAs catalyze the reversible aldol condensation of dihydroxyacetone phosphate (DHAP) with glyceraldehyde 3-phosphate (G3P) to form fructose 1,6-bisphosphate (FBP).[18] However, the two enzyme classes differ in their mechanism of catalysis and prevalence among species, which has made class II FBAs a

highly sought after bacterial target for pharmacological development. Specifically, class I FBAs utilize a lysine residue to generate a nucleophilic enamine from DHAP, whereas class II aldolases utilize a Zn(II) cation to stabilize the DHAP enolate intermediate involved in the aldol condensation reaction.[19] Also, the location of a key amino acid side chain responsible for proton extraction and addition significantly differs.[19–21] Beyond the differences in their reaction mechanisms, the two classes of FBAs distinctly differ in their distribution among species. Higher organisms such as humans possess only class I FBAs, whereas protozoa, bacteria, fungi, and blue-green algae primarily have class II FBAs, with a few possessing both.[22–24] In other words, selective inhibitors developed for class II FBAs are unlikely to generate toxic effects through disruption of the human class I FBA.

Additionally, the essentiality of class II FBAs within bacteria has been illustrated via knockout studies of both Gram-positive and Gram-negative bacteria, including M. tuberculosis, Escherichia coli, Streptomyces galbus, Bacillus subtilis, Pseudomonas aeruginosa, Streptococcus pneumoniae, and Candida albicans.[11,15,25–33] Although bacteria such as *E. coli* and other autotrophic prokaryotes possess both class I and class II FBAs, class I FBAs are only conditionally expressed, with class II FBAs being essential.[11,16,34,35] Beyond knockout studies and MtFBA being the only FBA in *M. tuberculosis*, MtFBA has been observed to be more abundantly produced and/or secreted by *M. tuberculosis* when placed in hypoxic conditions similar to those found within necrotic pulmonary lesions where *M. tuberculosis* resides.[7,17] A p-blast search also illustrates that MtFBA is 100% conserved across all sequenced strains of *M. tuberculosis*, including XDR-TB strain KZN605 as well as MDR-TB strain KZN1435. Taken together, the essentiality of class II FBAs and the absence of a human homologue have placed class II FBAs among the top potential bacterial drug targets currently lacking a viable preclinical drug candidate.

Naturally, as the essentiality of class II FBAs in bacteria was revealed in 2003, efforts began in earnest to develop class II FBA inhibitors for use as treatments related to TB and other bacterial and protozoan infections.[11] The first generation of these inhibitors began with the candidacy of a DHAP analogue, phosphoglycolohydroxymate (PGH) which was first reported in 1974.[9] Although PGH inhibits class II FBAs through competitive inhibition by mimicking DHAP, PGH is extremely promiscuous, inhibiting several mammalian enzymes, including class I FBAs.[8,36,37] Recent attempts to follow up on the competitive substrate mimicry approach utilized the chemical skeleton of FBP and focused on zinc–inhibitor interactions to gain greater specificity. Although low-micromolar, selective competitive inhibitors were observed for MtFBA and other bacterial class II FBAs, all of the inhibitors relied on the presence of one or two phosphate groups for selectivity and affinity.[6,8,9,12,13,23,38] Not surprisingly, with the presence of the highly charged phosphate moiety that likely interferes with transport across the cell membrane, only one of these substrate mimic-styled inhibitors has a measurable minimal inhibitory concentration (MIC) despite them being assessed up to 1 mM.[6,8,9,12,13,23,38] This sole exception is FBP analogue TD3 that possesses a 40 nM affinity for MtFBA. However, despite a recent attempt to validate or optimize TD3, no inhibitory effect on *M. tuberculosis* growth was observed, illustrating the limits of these types of inhibitors.[6,8]

Recently, we identified a chemical scaffold, 8-hydroxyquinoline-2-carboxylic acid (HCA), through the use of enzymatic and structure-based assisted screening that allows for selective, druglike, low-micromolar, noncompetitive inhibition of *M. tuberculosis* class IIa FBA as well as those from other pathogenic bacteria. To elucidate the *in vitro* characteristics of the interaction between HCA and MtFBA, the ability of HCA to inhibit MtFBA at multiple concentrations was examined, and isothermal titration calorimetry (ITC) was performed. Finally, an X-ray crystal structure of HCA bound with MtFBA was elucidated to 2.1 Å and compared to the apo and substrate-bound forms of MtFBA.

EXPERIMENTAL PROCEDURES

Materials

Chemicals, biochemicals, buffers, and solvents were purchased from Sigma-Aldrich Chemical Co. (St. Louis, MO), Fischer Scientific, Inc. (Pittsburgh, PA), Acros Organics (Morris Plains, NJ), or Worthington Biochemical Corp. (Lakewood, NJ) unless otherwise indicated. 8-Hydroxyquinoline-2-carboxylic acid (HCA) was purchased from Acros Organics (catalog no. 347620010). Enzymatic assay reagents, including bovine serum albumin (BSA, catalog no. A3059-50G), nicotinamide adenine dinucleotide hydrate (NAD^+, catalog no. 43407-25G), rabbit glyceraldehyde 3-phosphate dehydrogenase (GAPDH, catalog no. G2267-10KU), D-fructose 1,6-bisphosphate tetra-(cyclohexylammonium) salt (FBP, catalog no. F0752-5G), DL-glyceraldehyde 3-phosphate (G3P, catalog no. G5251-25MG), and dihydroxyacetone phosphate dilithium salt (DHAP, catalog no. D7137-100MG), were purchased from Sigma-Aldrich. Resazurin sodium salt was obtained from Acros Organics (catalog no. 189900250). Diaphorase was purchased from Worthington (catalog no. 4327). The Amicon Ultra-15 centrifugal filter devices were obtained from Millipore (UFC901024). The Ni-NTA and the Superdex-S200 High Resolution resins were obtained from Qiagen (Valencia, CA) and GE Healthcare, respectively. Recombinant human aldolase-A was obtained from GenWay Biotech, Inc. (San Diego, CA; GenWay catalog no. GWB-791DD1). Costar 96-well half-area, black flat-bottom polystyrene plates were purchased from Corning (catalog no. 3694).

Production and Purification of FBAs

The construction of the *M. tuberculosis* pET17b-*fba*H expression vector harboring the *fba* gene (Rv0363c) was performed as previously described.[15] The pET-*fba*H plasmid was introduced into *E. coli* BL21(DE3) by heat-shock transformation for enzyme expression. The resulting plasmid was then purified, restriction analyzed, and sequenced to verify the construct. The expression system produced a C-terminal, His-tagged fusion protein, which is herein termed MtFBA. Cells containing MtFBA were grown in 12 L of LB broth containing 100 μg/mL ampicillin until an OD_{600} of 0.6 was reached. Expression of the *fba*H gene was induced by addition of IPTG to a final concentration of 0.4 mM, and the culture was grown for an additional 4–6 h at 25 °C. Following this period, the bacterial cells were isolated via centrifugation at 3000*g* for 10 min and stored at −80 °C. The cell pellets were suspended in buffer A [300 mM NaCl and 50 mM Tris (pH 8.0)] and lysed by addition of 5 mg of chicken lysozyme followed by sonication. The insoluble cell debris was separated via centrifugation for 45 min at 17000*g*. MtFBA was purified from the resulting supernatant by using a Qiagen

Ni-NTA column and eluted with buffer A containing 300 mM imidazole followed by buffer exchange into buffer B [100 mM NaCl, 20 mM Tricine (pH 8.0), 2 mM DTT, and 0.1 mM $ZnCl_2$] by passage over a Superdex-S200 High Resolution column. The purified MtFBA was concentrated to 16 mg/mL via 10000 molecular weight cutoff centrifugal filter units (Millipore Cork, IRL) at 4000*g*. The final protein was then filtered through 0.22 μm Costar spin filters.

The production of the FBA expression vector for a methicillin-resistant strain of *Staphylococcus aureus* (SaFBA) was generated using *E. coli* BL21 optimized synthesis by Genscript, Inc. The SaFBA expression construct encodes the 289 amino acids from UniProtKB entry Q5HE75.1 as well as six histidines and a stop codon to generate a C-terminal histidine tag and incorporated them into pET11a plasmids using NdeI and BamHI restriction sites. Transformation, expression, and purification were performed in a manner similar to that of MtFBA.

The *E. coli* K-12 class II FBA was obtained from the ASKA library in a pCA24n-*fba*A expression vector harboring the *fba*A gene.[39] Transformation, expression, and purification were performed in a manner similar to that of MtFBA with the exception that 25 μg/mL chloramphenicol was used in place of ampicillin.

FBA purified from rabbit muscle was obtained as an ammonium sulfate suspension from Sigma-Aldrich (catalog no. A8811). The suspension was spun down at 13000*g* for 10 min at 4 °C, the supernatant discarded, and the pellet resuspended in buffer B supplemented with 1 mM EDTA. The resuspended protein was centrifuged again at 3000*g* for 15 min to remove any solids that remained.

Recombinant human aldolase-A was purchased form Gen-Way Biotech, Inc., at a concentration of 1 μg/μL in buffer C [20 mM Tris-HCl (pH 8.0), 100 mM NaCl, and 20% glycerol].

All protein concentrations were determined through UV–visible spectroscopy at 280 nm using molar extinction coefficients experimentally derived by the method of Gill and von Hippel.[40]

FBA Enzymatic FBP Cleavage Assays

The activity of FBAs was monitored through a fluorescence-based assay measuring the increase in fluorescence due to conversion of resazurin to resorufin via diaphorase when coupled with the oxidation of NADH to NAD^+. The assay mixture (final volume of 50 μL) contained 0.4 mM NAD^+, 8 units/mL GAPDH, 0.01% (w/v) BSA, 2 mM DTT, 15 mM NaH_2AsO_4, 100 mM Tris HCl (pH 7.8), 100 mM CH_3COOK, 180 nM MtTPI, 1 unit/μL diaphorase, and 50 μM resazurin. Triton X-100 was included at a final concentration of 0.01% in follow-up assays to identify any promiscuous inhibitors. For FBAs derived from *M. tuberculosis* and *E. coli*, a final assay concentration of 4 nM was used. For FBAs derived from *S. aureus*, rabbit, and human, a final assay concentration of 40 nM was used. The reaction was initiated via the addition of FBP at an assay concentration of 75 μM. All assays were performed at room temperature and in duplicate using Costar 96-well half-area, black

flat-bottom polystyrene plates (Corning). All FBA activity assays were conducted using a TECAN M1000 plate reader by measuring the fluorescence of resorufin at 585 nm when it was excited at 535 nm. A standard curve for FBP conversion was determined by adding excess MtFBA to various concentrations of FBP and allowing the reactions to run to completion. The resulting maximal fluorescence values were plotted to determine the slope and subsequently the conversion factor.

The IC_{50} value for the inhibition of MtFBA by HCA was determined at HCA concentrations ranging from 0 to 100 μM, with the FBP concentration held constant at 75 μM. The percent inhibition (*I*%) was calculated using the formula $I\% = [1 - (\nu_{sample} - \nu_{negative\ control})/(\nu_{positive\ control} - \nu_{negative\ control})] \times 100$. The resulting *I*% values were fit via nonlinear regression to the equation $I\% = I\%_{max}/(1 + IC_{50}/[HCA])$ using the Enzyme Kinetics Module of SigmaPlot, version 12.2 (SPSS, Inc.).

To determine the mode of action of HCA, inhibition studies were conducted using HCA concentrations ranging from 0 to 25 μM with four additional concentrations of FBP ranging from 9 to 150 μM used to initiate the reaction. Initial velocity data were fit using nonlinear regression analysis to each of the equations describing partial and full models of competitive, uncompetitive, noncompetitive, and mixed inhibition using the Enzyme Kinetics Module of SigmaPlot. On the basis of the analysis of fits through "goodness-of-fit" statistics, the full non-competitive inhibition model was determined with the equation $\nu = V_{max}/[(1 + [I]/K_i) \times (1 + K_m/[S])]$, where [S] = [FBP], [I] = [HCA], and K_i is the constant for dissociation of HCA from free MtFBA.

The class II FBAs from *E. coli* (4 nM) and *S. aureus* (40 nM) as well as the class I FBAs from rabbit muscle (40 nM) and human muscle (40 nM) were tested with a final HCA concentration of 25 μM. The reaction was initiated with 75 μM FBP, and I% was calculated as previously described.

Isothermal Titration Calorimetry (ITC) Experiments

ITC experiments were performed in duplicate using a NanoITC system (TA Instruments, Lindon, UT). MtFBA was dialyzed overnight at 4 °C against buffer D [100 mM NaCl, 20 mM Tricine (pH 8.0), and 2% DMSO]. HCA and $ZnCl_2$ were dissolved using the buffer in which MtFBA was dialyzed to concentrations of 5 and 10 mM, respectively. To assess the interaction between HCA and free zinc(II) ion, a solution of 5 mM HCA was titrated into 0.4 mM $ZnCl_2$. To assess the interaction between HCA and MtFBA, equal portions of 5 mM HCA and 10 mM $ZnCl_2$ were mixed and the HCA/$ZnCl_2$ mixture was titrated into 0.25 mM MtFBA. ITC runs were performed at 25 °C and comprised of one injection of 1 μL followed by 24 injections of 2 μL for a total of 25 injections. Each injection was spaced 200 s apart. The average heat released for the last five injections was used to correct for the heat of dilution. Data sets were analyzed with NanoAnalyze and fit to an independent model.

Inhibitor Susceptibility Testing

MIC values in 7H9-ADC-Tween 80 broth at 37 °C against *M. tuberculosis* H37Rv (avirulent strain mc^{2}6206) were determined using the resazurin blue assay[41] and by visually scanning for growth.

Crystallization of the MtFBA–HCA Complex

Initial crystallization conditions for the substrate-less, zinc-bound holo-MtFBA were achieved using conditions from our previously described protocols.[15] The final crystal was grown using hanging-drop vapor diffusion at 20 °C. Crystallization drops included 2 μL of a 16 mg/mL MtFBA protein solution containing buffer B mixed in a 1:1 ratio with 26% PEG 300, 0.1 M sodium acetate (pH 4.5), and 2% DMSO. After 4 weeks, the holo crystal was removed from the hanging drop, placed in 5 μL of a soaking solution containing 2.5 mM HCA, 26% PEG 300, 0.1 M sodium acetate (pH 4.5), and 2% DMSO for 1 h, and then flash-cooled in liquid nitrogen.

X-ray Structure of the the MtFBA–HCA Complex

An X-ray data set was collected using a crystal mounted onto a nylon loop flash-cooled in liquid nitrogen. The crystal was mounted under a stream of dry N_2 at 100 K. An MtFBA–HCA complex data set with resolution to 2.10 Å was collected at Advance Light Source (ALS) beamline 4.2.2 using a monochromic X-ray beam of 1.00 Å with a NOIR-1 MBC detector. X-ray images were indexed, processed, integrated, and scaled using HKL2000.[42] An initial phase solution was elucidated using holo-MtFBA [Protein Data Bank (PDB) entry 4DEF] as a starting model for molecular replacement using Phaser.[43] The structure was refined using iterative cycles of model building and refinement using COOT and phenix.refine, respectively.[44,45] Water molecules were added to $2F_o - F_c$ density peaks of >1σ using the Find Water COOT program function. The final model was checked for structural quality using the CCP4 suite programs Procheck and Sfcheck. The data refinement statistics are listed in Table 1.

Modeling Missing Loops into the Structure of the MtFBA–HCA Complex

Residues 167–177 and 210–223, which were unresolved in the X-ray crystal structure of MtFBA bound to HCA, were modeled in using MODELER 9v11 under default settings and the known sequence of MtFBA.[46] Five models were generated and inspected in PyMOL, and the final model was chosen by molpdf score.

RESULTS

Identification of HCA as an Inhibitor of MtFBA

Seeking an alternative to the substrate mimic-styled inhibitors that lack several qualities limiting their potential as viable preclinical leads for MtFBA and other class II FBAs, we adopted a fragment-based strategy. This strategy focused on enzymatically screening chemical moieties that would simulate the enolate transition state's hydroxamic acid of PGH with MtFBA's active site Zn(II) but be devoid of groups that would interfere with

pharmaceutical development. This set of compounds included several heterocyclic zinc binding groups that were used to screen for matrix metalloprotease inhibitors.[47–52]

Utilizing an assay that coupled MtFBA activity with *M. tuberculosis's* triosephosphate isomerase (TPI), rabbit glycerol-3-phosphate dehydrogenase (GAPDH), and diaphorase for a fluorescent output, 60 small molecules were screened in duplicate at a concentration of 1 mM. In addition to using a fluorophore that excited and emitted at wavelengths of >500 nm to prevent false positives, the assay also included DTT as well as BSA to ward off promiscuous inhibition.[53,54] This small, low-throughput screening campaign revealed that 8-hydroxyquinoline-2-carboxylic acid (HCA) reduced MtFBA activity more than 95% at a concentration of 1 mM.

Although several measures were taken to ward off promiscuous inhibition within the screening assay and reduce false positives, additional validation steps were conducted to further support HCA as a MtFBA inhibitor. Addition of Triton X-100, a known disruptor of aggregation-based inhibition, was introduced to test for any promiscuous inhibition, with no alteration in potency observed (Figure 1a).[54] Despite the coupling enzymes already being in >40-fold excess, to further rule out the possibility that HCA was inhibiting a coupling enzyme instead of MtFBA, a 160-fold excess of each coupling enzyme was added and assessed at a HCA concentration of 25 μM (Figure 1a). No ablation of HCA inhibition was observed, suggesting HCA's effect on the assay was linked specifically to MtFBA inhibition. Also, as expected, no HCA-facilitated inhibition of the assay was detected when MtFBA's assay products DHAP and G3P were substituted for MtFBA. Understandably, there have been numerous reports of compounds possessing 8-hydroxyquinoline moieties acting as promiscuous chelating agents.[49,55,56] To test this possibility, a 2-fold increase in the level of Zn(II) was used to determine if HCA was indirectly inhibiting MtFBA activity by sequestering Zn(II) in solution. If HCA was limiting MtFBA's access to Zn(II), or stripping MtFBA of Zn(II), an increase in the level of Zn(II) should reduce the inhibitory effects of HCA on MtFBA activity. Unexpectedly, the potency of HCA for MtFBA slightly increased (Figure 1a). A dose–response relationship of HCA and MtFBA conducted under these conditions yielded an IC_{50} of 10 ± 1 μM (Figure 1b). Importantly, HCA inhibited the growth of *M. tuberculosis* in 7H9-OADC broth at a concentration of 0.6–1.2 mM.

Biochemical and Biophysical Properties of the MtFBA–HCA Interaction

To characterize the nature of the inhibition of MtFBA by HCA, kinetic studies and ITC experiments were conducted. To understand the mechanism of inhibition of MtFBA activity by HCA, five different FBP concentrations and six different HCA concentrations were utilized to determine the kinetic response of MtFBA to varying concentrations of substrate and inhibitor. Surprisingly, only the V_{max} of MtFBA was significantly affected over a 20-fold increase in inhibitor concentration, whereas the K_M remained constant (Figure 1c). This along with using nonlinear regression analysis indicated that HCA acts in a noncompetitive manner against FBP with a K_i of 12 ± 1 μM, instead of a competitive manner like previously characterized class II FBA inhibitors. Next, as HCA is known to bind to zinc (II), the biophysical binding characteristics of HCA and free zinc (II) in solution were analyzed via ITC. This revealed an exothermic binding event with the following values: K_d = 9.39 ± 0.79

μM, ΔH = −26.8 ± 0.3 kJ/mol, ΔS = 6.9 ± 0.9 J mol^{-1} K^{-1}, and n = 1.86 ± 0.10 (Figure 2a). The binding stoichiometry of HCA and free zinc (II) in solution determined by ITC matches current X-ray crystallography data for the structure of HCA bound to free zinc (II), which also showed HCA and zinc (II) interacting in a ratio of 2:1.[55] Intriguingly, the data from the enzymatic assay showed that HCA's inhibitory effects against MtFBA are not reduced in the presence of a 2-fold excess of $ZnCl_2$. Therefore, to assess the thermodynamic factors that may favor HCA's interaction with MtFBA versus free zinc (II), HCA was first combined with a 3-fold excess of $ZnCl_2$ required for the formation of the HCA–free zinc (II) complex and then titrated into MtFBA. As Pegan et al. and de la Paz Santangelo et al. recently reported that zinc (II) has to be in solution for the active site of MtFBA to be fully occupied, the presence of excess zinc (II) ensured full occupancy.[7,14] In addition, the excess zinc allows for the observation of thermodynamic contributions outside of HCA–zinc (II) binding events whether with free zinc (II) in solution or the active site zinc of MtFBA. Interestingly, the binding profile of HCA with excess $ZnCl_2$ in MtFBA differed from that of HCA and free zinc (II), resulting in the following values: K_d = 70.8 ± 2.7 μM, ΔH = −66.0 ± 1.0 kJ/mol, ΔS = −141.9 ± 3.2 J mol^{-1} K^{-1}, and n = 0.96 ± 0.01 (Figure 2b). This suggests that additional enthalpic forces are present within the interaction between HCA and MtFBA and may be responsible for HCA's ability to inhibit MtFBA in a direct manner.

Determination of the Structure of HCA Bound to MtFBA

With the biochemical data proposing that HCA acts in a manner unlike that of current class II inhibitors of MtFBA, the X-ray crystallographic structure of HCA bound to MtFBA (MtFBA–HCA) was sought. Utilizing previous techniques to generate MtFBA in its zinc (II)-bound but substrate-less (holo-MtFBA) form, these crystals were soaked in HCA.[14] A crystal structure of these HCA-soaked crystals was subsequently resolved to 2.1 Å (Table 1). Not surprisingly, the single monomer in the asymmetric unit globally mirrored the TIM barrel fold of previous MtFBA structures and formed a tetrameric biological assembly with monomers from adjoining asymmetric units (Figures 3 and 4a). However, unlike the fully elucidated MtFBA–PGH structure that possessed density for the entire protein, two regions lacked electron density in the MtFBA–HCA structure (Figure 4a,b). One of these regions is the highly flexible active site loop comprised of amino acids 167–177, which contains Glu169 required for the deprotonation–protonation step of the MtFBA-facilitated reaction.[14] The absence of this loop was not particularly shocking as it has been resolved in only one class II FBA structure, that of MtFBA bound to PGH.[14] Conversely, the second region of MtFBA missing electron density, which encompassed the β6α6 loop containing residues 210–223, was unusual. This loop forms part of the substrate pocket and contains His212, whose imidazole side chain is involved in coordinating the active site Zn(II) ion and can be considered the zinc binding loop [Z-loop (Figure 4c)].[14]

Subsequently, closer inspection of the region where the Z-loop would typically reside, as well as the active site, readily revealed $F_o - F_c$ density of HCA coordinating the MtFBA's active site Zn(II) in a trident manner (Figure 5a and Figure S1 of the Supporting Information). Intriguingly, instead of accessing the active site Zn(II) through the highly polar and narrow substrate pocket of MtFBA, HCA appears to alter the active site. Specifically, it displaces the His212's imidazole side chain for the bound Zn(II). This creates

a hydrophobic pocket that accommodates the bicyclic structure of HCA (Figure 5b). In addition to the displacement of His212, Val165, which is located on the flexible active site β5α5 loop, is also supplanted by HCA (Figure 5b).[14] Although the X-ray data showed clear density for Val165, its position was shifted away from the active site. Beyond these alterations with the MtFBA active site, HCA forms three coordination bonds with Zn(II). As observed in previous MtFBA structures, two additional coordination bonds are formed between Zn(II) and histidine residues located at positions 96 and 252. Together, these interactions yield a coordination number of 5 (T_5) for the active site Zn similar to that of the PGH bound and different from the T_6 coordination found in the FBP structure (Figure 5a–c).[15] In addition to the Zn(II)–HCA interactions, HCA forms a hydrogen bond (H-bond) with Glu161 of MtFBA as well as a network of H-bonds through water to Asp95 that further drives HCA stabilization within the altered active site (Figure 5a).

Examining HCA's Specificity for Class I and II FBAs

As class II FBAs share considerable sequence similarity (Figure 3a), HCA's potential as a class II FBA broad-spectrum inhibitor was examined. A single concentration of HCA of 25 μM was tested for the inhibition of class II FBAs isolated from *E. coli* and methicillin-resistant *S. aureus* (MRSA). HCA demonstrated 42.2 ± 2.8% inhibition against *E. coli* and 64.3 ± 0.6% inhibition against MRSA (Figure 6). Conversely, class I FBAs are markedly different in sequence from class II FBAs and do not utilize a zinc (II) ion to perform their mechanistic function. Therefore, to investigate HCA's specificity for class II FBAs over class I FBAs, the class I FBAs isolated from both rabbit and human muscle were tested against HCA. Unlike class II FBAs, HCA showed no inhibitory effects against either class I FBA even at concentrations as high as 1 mM (Figure 6).

DISCUSSION

HCA as a Noncompetitive MtFBA Inhibitor

The alignment of the MtFBA–HCA structure with those of MtFBA bound with FBP, or PGH, illustrates that HCA does not intrude into the substrate pocket itself (Figure 5b,c). Instead, incorporation of HCA into MtFBA appears to displace the Z-loop and in doing so blocks access of MtFBA substrates to an empty pocket (Figure 5b,c). The proximity of a noncompetitive inhibitor to a substrate pocket has been previously observed with a noncompetitive inhibitor, PD184352, of MAP kinase kinase 1 (MEK1).[57] The noncompetitive nature of inhibition outlined by the mode of inhibition experiments combined with the structural data suggests that the MtFBA–HCA structure may be reflective of an EI complex found in the third model for noncompetitive inhibition (Figure 7a).[58] In this model, the inhibitor binds next to the substrate binding site with or without the substrate bound. When the substrate is absent, the inhibitor sterically hinders access of substrates to an empty site comparable to that observed in the structure of the MtFBA–HCA complex (Figure 7a). Also, the myriad of coordination bonds and H-bonds that HCA forms with MtFBA pulls the Zn(II) away from the substrate binding pocket. This would likely eliminate its availability for catalysis in an ESI complex in line with the third model of noncompetitive inhibition.

Use of HCA as a Scaffold for Future MtFBA Inhibitor Development

The persistence of tuberculosis along with the rise of many forms of drug resistant bacteria has supported the interest in identifying inhibitors for class II FBAs that may serve as viable preclinical candidates for further development as antibiotic and antiparasitic treatments.[6–9,12–14,38] Although previous class II FBA inhibitor development efforts have been able to deliver potent substrate-based analogs selective for class II over class I FBAs, the recurring theme throughout studies utilizing class II FBA substrates as a scaffold is the necessity of these inhibitors to possess highly charged phosphate groups.[8,13,38] As phosphorylation of glycolytic intermediates is a method for cells to retain these intermediates within the cytosol, their inclusion into class II FBA inhibitors has been problematic.[59] In addition, the active site of class II FBA, which has evolved to interact with class II FBA's highly polar substrates, is itself highly polar, lacking appreciable potential for hydrophobic interactions. As this form of interaction typically dominates protein–drug interactions, targeting the class II FBA active site has proved to be daunting.

HCA sidesteps both of these issues through its distinct low-micromolar noncompetitive mode of inhibiting MtFBA. Specifically, HCA appears to take advantage of the previously overlooked fragility of the coordination of His212 of MtFBA with Zn(II) along with the structural dependence of the Z-loop on that interaction to facilitate hydrophobic and hydrophilic contacts. At first glance, the substrate- and Zn(II)-bound MtFBA structures of Pegan et al.,[15] as well as the Zn(II)-bound holo-MFBA structure of Pegan et al.,[14] might have suggested that a stable interaction between His212 and an active site Zn(II) potentially existed. In addition, a zinc-less MtFBA apo structure of de la Paz Santangelo et al.[7] illustrates that the ordered structure of the Z-loop depends on the presence of Zn(II) within the active site. However, the MtFBA–HCA structure suggests that even when Zn(II) is bound to the MtFBA active site, the interaction between His212 and the bound Zn(II) is still in flux. This flux allows HCA to supplant His212 with a trident coordination of the metal or a HCA–Zn(II) complex to replace the active site Zn(II). Naturally, additional experiments will likely be necessary to tease out which event is more likely. However, the MtFBA–HCA structure along with the biochemical and biophysical experiments illustrates that HCA prefers to be bound to MtFBA's active site Zn(II) and that this Zn(II) prefers HCA over His212.

From the MtFBA–HCA structure, this preference appears to be driven by not only a H-bond network formed by bonds from HCA to Asp95 and Glu161 of MtFBA that pulls Zn(II) away from the active site, but also hydrophobic interactions caused by the creation of a hydrophobic pocket that accommodates HCA's bicyclic ring structure (Figure 5b). As hydrophobic interactions are usually sought for protein–drug interactions and are a largely insignificant factor in the affinity of previous inhibitors for class II FBAs, the presence of this feature in MtFBA–HCA interactions is particularly noteworthy. In addition to HCA's distinct mode of inhibition, HCA possesses several features that make the compound attractive from a medicinal chemistry perspective. First, the compound has a low molecular mass of 189 Da and contains minimal structural features. Furthermore, functionality can be added at a variety of places on HCA while still likely maintaining druglike properties.[53,60,61] Also, HCA appears via the MtFBA–HCA structure to capitalize on the unique mechanistic

difference between class I and class II FBAs by interacting with MtFBA active site zinc and residues immediately surrounding it. These residues along with Zn^{2+} do not exist in class I FBAs. This combined with the lack of measurable inhibition of mammalian class I FBAs suggests the HCA scaffold could represent a significant leap forward in class II FBA preclinical inhibitor development.

Broad-Spectrum Potential of HCA

Interestingly, class II FBAs can be broken down into two families (a and b) whose distribution among bacterium is independent of Gram staining-determined phylogenetic groups. Naturally, all class II FBAs have an evolutionary need to maintain an effective active site that binds Zn(II) and a common set of substrates. As a result, the structural differences between these two subfamilies are predominantly distal from their respective active sites and are involved in determining the diverse oligomeric states adopted by class II FBAs.[15] This phenomenon is well-represented upon comparison of residues that comprise the HCA-induced pocket (Figure 7b). Structural alignments of class IIa FBAs from *M. tuberculosis* and *E. coli* along with that of *B. anthracis*'s class IIb FBA reinforce the potentially conserved nature of the HCA-induced pocket (Figure 7b). The ability of HCA to significantly inhibit both the class IIa FBA from *E. coli* and a class IIb FBA from MRSA further supports the potential use of the HCA scaffold for these bacteria. Of course, additional experiments with these or other class II FBAs will have to be conducted to fully confirm HCA is acting in a manner similar to that observed in MtFBA. However, the initial evidence bodes well for the broad-spectrum potential of the HCA scaffold in further class II FBA preclinical inhibitor design efforts.

Supplementary Material

Refer to Web version on PubMed Central for supplementary material.

Acknowledgments

We thank Mrs. Victoria Jones for her help with determination of MICs as well as Dr. Alexander Mankin (University of Illinois, Chicago, IL) for generously providing expression vector pCA24n-*fba*A harboring the *fbaA* gene from *E. coli* K-12. Also, we thank Dr. Den R. Tolan (Boston University, Boston, MA) for generously donating the Sigma-Aldrich rabbit class I FBA. Marvin was used for drawing, displaying, and characterizing chemical structures, substructures, and reactions [Marvin 5.5.1.0, 2013, ChemAxon (http://www.chemaxon.com)].

Funding This research was supported in part by grants from the Professional Research Opportunities for Faculty (S.D.P.), the Colorado Center for Drug Discovery (S.D.P. and K.A.A.), Cancer Center Support Grant P30CA046934 (S.D.P.), and the Regis University Research and Scholarship Council (K.A.A.). The Advanced Light Source is supported by the Director, Office of Science, Office of Basic Energy Sciences, of the U.S. Department of Energy under Contract DE-AC02-05CH11231.

ABBREVIATIONS

ALS	Advanced Light Source
BSA	bovine serum albumin
DHAP	dihydroxyacetone phosphate
DMSO	dimethyl sulfoxide

DOTS	Directly Observed Therapy, Short Course
DTT	dithiothreitol
EcFBA	*E. coli* class II fructose 1,6-bisphosphate aldolase
FBP	fructose 1,6-bisphosphate
GAPDH	glyceraldehyde-3-phosphate dehydrogenase
G3P	glyceraldehyde 3-phosphate
HCA	8-hydroxyquinoline-2-carboxylic acid
HEPES	*N*-(2-hydroxyethyl)piperazine-*N*′-2-ethanesulfonate
ITC	isothermal titration calorimetry
IPTG	isopropyl β-D-thiogalactoside
LB	Luria-Bertani
MIC	minimal inhibitory concentration
MRSA	methicillin-resistant *S. aureus*
MDR-TB	multidrug-resistant tuberculosis
MtFBA	*M. tuberculosis* class II fructose 1,6-bisphosphate aldolase
NAD^+	nicotinamide adenine dinucleotide
NADH	reduced nicotinamide adenine dinucleotide
Ni-NTA	nickel-nitrilotriacetic acid
PEG	polyethylene glycol
PCR	polymerase chain reaction
PGH	phosphoglycolohydroxamate
SaFBA	*S. aureus* class II fructose 1,6-bisphosphate aldolase
SDS–PAGE	sodium dodecyl sulfate–polyacrylamide gel electrophoresis
TPI	triosephosphate isomerase
TB	tuberculosis
WHO	World Health Organization
XRD-TB	extensively drug-resistant tuberculosis

REFERENCES

(1). World Health Organization. Global tuberculossis control: Surveillance, planning, financing. World Health Organization; Geneva: 2008.

(2). World Health Organization. Global tuberculosis report 2012 (in IRIS). World Health Organization; Geneva: 2012.

(3). World Health Organization. UNAIDS, and UNICEF. Global HIV/AIDS response: Epidemic update and health sector progress towards universal access: Progress report 2011. World Health Organization; Geneva: 2011.

(4). World Health Organization. Implementing the Stop TB Strategy: A handbook for national tuberculosis. World Health Organization; Geneva: 2008.

(5). World Health Organization. Tuberculosis MDR-TB & XDR-TB. World Health Organization; Geneva: 2008.

(6). Daher R, Coincon M, Fonvielle M, Gest PM, Guerin ME, Jackson M, Sygusch J, Therisod M. Rational design, synthesis, and evaluation of new selective inhibitors of microbial class II (zinc dependent) fructose bis-phosphate aldolases. J. Med. Chem. 2010; 53:7836–7842. [PubMed: 20929256]

(7). de la Paz Santangelo M, Gest PM, Guerin ME, Coincon M, Pham H, Ryan G, Puckett SE, Spencer JS, Gonzalez-Juarrero M, Daher R, Lenaerts AJ, Schnappinger D, Therisod M, Ehrt S, Sygusch J, Jackson M. Glycolytic and non-glycolytic functions of *Mycobacterium tuberculosis* fructose-1,6-bisphosphate aldolase, an essential enzyme produced by replicating and non-replicating bacilli. J. Biol. Chem. 2011; 286:40219–40231. [PubMed: 21949126]

(8). Fonvielle M, Coincon M, Daher R, Desbenoit N, Kosieradzka K, Barilone N, Gicquel B, Sygusch J, Jackson M, Therisod M. Synthesis and biochemical evaluation of selective inhibitors of class II fructose bisphosphate aldolases: Towards new synthetic antibiotics. Chemistry. 2008; 14:8521–8529. [PubMed: 18688832]

(9). Fonvielle M, Weber P, Dabkowska K, Therisod M. New highly selective inhibitors of class II fructose-1,6-bisphosphate aldolases. Bioorg. Med. Chem. Lett. 2004; 14:2923–2926. [PubMed: 15125960]

(10). Galkin A, Li Z, Li L, Kulakova L, Pal LR, Dunaway-Mariano D, Herzberg O. Structural insights into the substrate binding and stereoselectivity of Giardia fructose-1,6-bisphosphate aldolase. Biochemistry. 2009; 48:3186–3196. [PubMed: 19236002]

(11). Gerdes SY, Scholle MD, Campbell JW, Balazsi G, Ravasz E, Daugherty MD, Somera AL, Kyrpides NC, Anderson I, Gelfand MS, Bhattacharya A, Kapatral V, D'Souza M, Baev MV, Grechkin Y, Mseeh F, Fonstein MY, Overbeek R, Barabasi AL, Oltvai ZN, Osterman AL. Experimental determination and system level analysis of essential genes in Escherichia coli MG1655. J. Bacteriol. 2003; 185:5673–5684. [PubMed: 13129938]

(12). Labbe G, Krismanich AP, de Groot S, Rasmusson T, Shang M, Brown MD, Dmitrienko GI, Guillemette JG. Development of metal-chelating inhibitors for the Class II fructose 1,6-bisphosphate (FBP) aldolase. J. Inorg. Biochem. 2012; 112:49–58. [PubMed: 22546686]

(13). Li Z, Liu Z, Cho DW, Zou J, Gong M, Breece RM, Galkin A, Li L, Zhao H, Maestas GD, Tierney DL, Herzberg O, Dunaway-Mariano D, Mariano PS. Rational design, synthesis and evaluation of first generation inhibitors of the *Giardia lamblia* fructose-1,6-biphosphate aldolase. J. Inorg. Biochem. 2011; 105:509–517. [PubMed: 21333622]

(14). Pegan SD, Rukseree K, Capodagli GC, Baker EA, Krasnykh O, Franzblau SG, Mesecar AD. Active site loop dynamics of a class IIa fructose 1,6-bisphosphate aldolase from *Mycobacterium tuberculosis*. Biochemistry. 2013; 52:912–925. [PubMed: 23298222]

(15). Pegan SD, Rukseree K, Franzblau SG, Mesecar AD. Structural basis for catalysis of a tetrameric class IIa fructose 1,6-bisphosphate aldolase from *Mycobacterium tuberculosis*. J. Mol. Biol. 2009; 386:1038–1053. [PubMed: 19167403]

(16). Ramsaywak PC, Labbe G, Siemann S, Dmitrienko GI, Guillemette JG. Molecular cloning, expression, purification, and characterization of fructose 1,6-bisphosphate aldolase from *Mycobacterium tuberculosis*: A novel Class II A tetramer. Protein Expression Purif. 2004; 37:220–228.

(17). Rosenkrands I, Slayden RA, Crawford J, Aagaard C, Barry CE III, Andersen P. Hypoxic response of *Mycobacterium tuberculosis* studied by metabolic labeling and proteome analysis of cellular and extracellular proteins. J. Bacteriol. 2002; 184:3485–3491. [PubMed: 12057942]

(18). Rutter WJ. Evolution of Aldolase. Fed. Proc. 1964; 23:1248–1257. [PubMed: 14236133]

(19). Pegan SD, Rukseree K, Franzblau SG, Mesecar AD. Structural Basis for Catalysis of a Tetrameric Class IIa Fructose 1,6-Bisphosphate Aldolase from Mycobacterium tuberculosis. J. Mol. Biol. 2009; 386:1038–1053. [PubMed: 19167403]

(20). Zgiby S, Plater AR, Bates MA, Thomson GJ, Berry A. A functional role for a flexible loop containing Glu182 in the class II fructose-1,6-bisphosphate aldolase from Escherichia coli. J. Mol. Biol. 2002; 315:131–140. [PubMed: 11779234]

(21). Lorentzen E, Siebers B, Hensel R, Pohl E. Mechanism of the Schiff base forming fructose-1,6-bisphosphate aldolase: Structural analysis of reaction intermediates. Biochemistry. 2005; 44:4222–4229. [PubMed: 15766250]

(22). Izard T, Sygusch J. Induced fit movements and metal cofactor selectivity of class II aldolases: Structure of *Thermus aquaticus* fructose-1,6-bisphosphate aldolase. J. Biol. Chem. 2004; 279:11825–11833. [PubMed: 14699122]

(23). Galkin A, Kulakova L, Melamud E, Li L, Wu C, Mariano P, Dunaway-Mariano D, Nash TE, Herzberg O. Characterization, kinetics, and crystal structures of fructose-1,6-bisphosphate aldolase from the human parasite. Giardia lamblia. J. Biol. Chem. 2007; 282:4859–4867.

(24). Marsh JJ, Lebherz HG. Fructose-bisphosphate aldolases: An evolutionary history. Trends Biochem. Sci. 1992; 17:110–113. [PubMed: 1412694]

(25). Baba T, Ara T, Hasegawa M, Takai Y, Okumura Y, Baba M, Datsenko KA, Tomita M, Wanner BL, Mori H. Construction of *Escherichia coli* K-12 in-frame, single-gene knockout mutants: The Keio collection. Mol. Syst. Biol. 2006; 2 2006.0008.

(26). Giaever G, Chu AM, Ni L, Connelly C, Riles L, Veronneau S, Dow S, Lucau-Danila A, Anderson K, Andre B, Arkin AP, Astromoff A, El-Bakkoury M, Bangham R, Benito R, Brachat S, Campanaro S, Curtiss M, Davis K, Deutschbauer A, Entian KD, Flaherty P, Foury F, Garfinkel DJ, Gerstein M, Gotte D, Guldener U, Hegemann JH, Hempel S, Herman Z, Jaramillo DF, Kelly DE, Kelly SL, Kotter P, LaBonte D, Lamb DC, Lan N, Liang H, Liao H, Liu L, Luo C, Lussier M, Mao R, Menard P, Ooi SL, Revuelta JL, Roberts CJ, Rose M, Ross-Macdonald P, Scherens B, Schimmack G, Shafer B, Shoemaker DD, Sookhai-Mahadeo S, Storms RK, Strathern JN, Valle G, Voet M, Volckaert G, Wang CY, Ward TR, Wilhelmy J, Winzeler EA, Yang Y, Yen G, Youngman E, Yu K, Bussey H, Boeke JD, Snyder M, Philippsen P, Davis RW, Johnston M. Functional profiling of the *Saccharomyces cerevisiae genome*. Nature. 2002; 418:387–391. [PubMed: 12140549]

(27). Jacobs MA, Alwood A, Thaipisuttikul I, Spencer D, Haugen E, Ernst S, Will O, Kaul R, Raymond C, Levy R, Chun-Rong L, Guenthner D, Bovee D, Olson MV, Manoil C. Comprehensive transposon mutant library of *Pseudomonas aeruginosa*. Proc. Natl. Acad. Sci. U.S.A. 2003; 100:14339–14344. [PubMed: 14617778]

(28). Kobayashi K, Ehrlich SD, Albertini A, Amati G, Andersen KK, Arnaud M, Asai K, Ashikaga S, Aymerich S, Bessieres P, Boland F, Brignell SC, Bron S, Bunai K, Chapuis J, Christiansen LC, Danchin A, Debarbouille M, Dervyn E, Deuerling E, Devine K, Devine SK, Dreesen O, Errington J, Fillinger S, Foster SJ, Fujita Y, Galizzi A, Gardan R, Eschevins C, Fukushima T, Haga K, Harwood CR, Hecker M, Hosoya D, Hullo MF, Kakeshita H, Karamata D, Kasahara Y, Kawamura F, Koga K, Koski P, Kuwana R, Imamura D, Ishimaru M, Ishikawa S, Ishio I, Le Coq D, Masson A, Mauel C, Meima R, Mellado RP, Moir A, Moriya S, Nagakawa E, Nanamiya H, Nakai S, Nygaard P, Ogura M, Ohanan T, O'Reilly M, O'Rourke M, Pragai Z, Pooley HM, Rapoport G, Rawlins JP, Rivas LA, Rivolta C, Sadaie A, Sadaie Y, Sarvas M, Sato T, Saxild HH, Scanlan E, Schumann W, Seegers JF, Sekiguchi J, Sekowska A, Seror SJ, Simon M, Stragier P, Studer R, Takamatsu H, Tanaka T, Takeuchi M, Thomaides HB, Vagner V, van Dijl JM, Watabe K, Wipat A, Yamamoto H, Yamamoto M, Yamamoto Y, Yamane K, Yata K, Yoshida K, Yoshikawa H, Zuber U, Ogasawara N. Essential *Bacillus subtilis* genes. Proc. Natl. Acad. Sci. U.S.A. 2003; 100:4678–4683. [PubMed: 12682299]

(29). Liberati NT, Urbach JM, Miyata S, Lee DG, Drenkard E, Wu G, Villanueva J, Wei T, Ausubel FM. An ordered, nonredundant library of *Pseudomonas aeruginosa* strain PA14 transposon insertion mutants. Proc. Natl. Acad. Sci. U.S.A. 2006; 103:2833–2838. [PubMed: 16477005]

(30). Rodaki A, Young T, Brown AJ. Effects of depleting the essential central metabolic enzyme fructose-1,6-bisphosphate aldolase on the growth and viability of *Candida albicans*: Implications for antifungal drug target discovery. Eukaryotic Cell. 2006; 5:1371–1377. [PubMed: 16896220]

(31). Sassetti CM, Boyd DH, Rubin EJ. Genes required for mycobacterial growth defined by high density muta-genesis. Mol. Microbiol. 2003; 48:77–84. [PubMed: 12657046]

(32). Song JH, Ko KS, Lee JY, Baek JY, Oh WS, Yoon HS, Jeong JY, Chun J. Identification of essential genes in *Streptococcus pneumoniae* by allelic replacement mutagenesis. Mol. Cells. 2005; 19:365–374. [PubMed: 15995353]

(33). Wehmeier UF. Molecular cloning, nucleotide sequence and structural analysis of the *Streptomyces galbus* DSM40480 fda gene: The *S. galbus* fructose-1,6-bisphosphate aldolase is a member of the class II aldolases. FEMS Microbiol. Lett. 2001; 197:53–58. [PubMed: 11287146]

(34). Stribling D, Perham RN. Purification and characterization of two fructose diphosphate aldolases from *Escherichia coli* (Crookes' strain). Biochem. J. 1973; 131:833–841. [PubMed: 4198624]

(35). Scamuffa MD, Caprioli RM. Comparison of the mechanisms of two distinct aldolases from *Escherichia coli* grown on gluconeogenic substrates. Biochim. Biophys. Acta. 1980; 614:583–590. [PubMed: 6996735]

(36). Collins KD. An activated intermediate analogue. The use of phosphoglycolohydroxamate as a stable analogue of a transiently occurring dihydroxyacetone phosphate-derived enolate in enzymatic catalysis. J. Biol. Chem. 1974; 249:136–142. [PubMed: 4588689]

(37). Dreyer MK, Schulz GE. Catalytic mechanism of the metal-dependent fuculose aldolase from *Escherichia coli* as derived from the structure. J. Mol. Biol. 1996; 259:458–466. [PubMed: 8676381]

(38). Gavalda S, Braga R, Dax C, Vigroux A, Blonski C. N-Sulfonyl hydroxamate derivatives as inhibitors of class II fructose-1,6-diphosphate aldolase. Bioorg. Med. Chem. Lett. 2005; 15:5375–5377. [PubMed: 16236509]

(39). Kitagawa M, Ara T, Arifuzzaman M, Ioka-Nakamichi T, Inamoto E, Toyonaga H, Mori H. Complete set of ORF clones of *Escherichia coli* ASKA library (a complete set of *E. coli* K-12 ORF archive): Unique resources for biological research. DNA Res. 2005; 12:291–299. [PubMed: 16769691]

(40). Gill SC, von Hippel PH. Calculation of protein extinction coefficients from amino acid sequence data. Anal. Biochem. 1989; 182:319–326. [PubMed: 2610349]

(41). Martin A, Camacho M, Portaels F, Palomino JC. Resazurin microtiter assay plate testing of *Mycobacterium tuberculosis* susceptibilities to second-line drugs: Rapid, simple, and inexpensive method. Antimicrob. Agents Chemother. 2003; 47:3616–3619. [PubMed: 14576129]

(42). Otwinowski, Z.; Minor, W. Macro-molecular Crystallography, Part A. Vol. 276. Academic Press; New York: 1997. Processing of X-ray Diffraction Data Collected in Oscillation Mode.

(43). Bailey S. The Ccp4 Suite: Programs for Protein Crystallography. Acta Crystallogr. 1994; D50:760–763.

(44). Emsley P, Cowtan K. Coot: Model-building tools for molecular graphics. Acta Crystallogr. 2004; D60:2126–2132.

(45). Adams PD, Afonine PV, Bunkoczi G, Chen VB, Davis IW, Echols N, Headd JJ, Hung LW, Kapral GJ, Grosse-Kunstleve RW, McCoy AJ, Moriarty NW, Oeffner R, Read RJ, Richardson DC, Richardson JS, Terwilliger TC, Zwart PH. PHENIX: A comprehensive Python-based system for macromolecular structure solution. Acta Crystallogr. 2010; D66:213–221.

(46). Sali A, Blundell TL. Comparative Protein Modeling by Satisfaction of Spatial Restraints. J. Mol. Biol. 1993; 234:779–815. [PubMed: 8254673]

(47). Agrawal A, Johnson SL, Jacobsen JA, Miller MT, Chen LH, Pellecchia M, Cohen SM. Chelator fragment libraries for targeting metalloproteinases. ChemMedChem. 2010; 5:195–199. [PubMed: 20058293]

(48). Agrawal A, Romero-Perez D, Jacobsen JA, Villarreal FJ, Cohen SM. Zinc-binding groups modulate selective inhibition of MMPs. ChemMedChem. 2008; 3:812–820. [PubMed: 18181119]

(49). Jacobsen JA, Fullagar JL, Miller MT, Cohen SM. Identifying chelators for metalloprotein inhibitors using a fragment-based approach. J. Med. Chem. 2011; 54:591–602. [PubMed: 21189019]

(50). Puerta DT, Griffin MO, Lewis JA, Romero-Perez D, Garcia R, Villarreal FJ, Cohen SM. Heterocyclic zinc-binding groups for use in next-generation matrix metalloproteinase inhibitors: Potency, toxicity, and reactivity. J. Biol. Inorg. Chem. 2006; 11:131–138. [PubMed: 16391944]

(51). Puerta DT, Lewis JA, Cohen SM. New beginnings for matrix metalloproteinase inhibitors: Identification of high-affinity zinc-binding groups. J. Am. Chem. Soc. 2004; 126:8388–8389. [PubMed: 15237990]

(52). Rouffet M, de Oliveira CA, Udi Y, Agrawal A, Sagi I, McCammon JA, Cohen SM. From sensors to silencers: Quinoline- and benzimidazole-sulfonamides as inhibitors for zinc proteases. J. Am. Chem. Soc. 2010; 132:8232–8233. [PubMed: 20507095]

(53). Lipinski CA, Lombardo F, Dominy BW, Feeney PJ. Experimental and computational approaches to estimate solubility and permeability in drug discovery and development settings. Adv. Drug Delivery Rev. 2001; 46:3–26.

(54). Feng BY, Shoichet BK. A detergent-based assay for the detection of promiscuous inhibitors. Nat. Protoc. 2006; 1:550–553. [PubMed: 17191086]

(55). McDonald FC, Applefield RC, Halkides CJ, Reibenspies JH, Hancock RD. A thermodynamic and crystallo-graphic study of complexes of the highly preorganized ligand 8-hydroxyquinoline-2-carboxylic acid. Inorg. Chim. Acta. 2008; 361:1937–1946.

(56). Sobke A, Klinger M, Hermann B, Sachse S, Nietzsche S, Makarewicz O, Keller PM, Pfister W, Straube E. The urinary antibiotic 5-nitro-8-hydroxyquinoline (Nitroxoline) reduces the formation and induces the dispersal of *Pseudomonas aeruginosa* biofilms by chelation of iron and zinc. Antimicrob. Agents Chemother. 2012; 56:6021–6025. [PubMed: 22926564]

(57). Ohren JF, Chen H, Pavlovsky A, Whitehead C, Zhang E, Kuffa P, Yan C, McConnell P, Spessard C, Banotai C, Mueller WT, Delaney A, Omer C, Sebolt-Leopold J, Dudley DT, Leung IK, Flamme C, Warmus J, Kaufman M, Barrett S, Tecle H, Hasemann CA. Structures of human MAP kinase kinase 1 (MEK1) and MEK2 describe novel noncompetitive kinase inhibition. Nat. Struct. Mol. Biol. 2004; 11:1192–1197. [PubMed: 15543157]

(58). Segel, IH. Enzyme kinetics: Behavior and analysis of rapid equilibrium and steady state enzyme systems. Wiley; New York: 1975.

(59). Lehninger, A.; Nelson, D.; Cox, M. Lehninger Principles of Biochemistry. W. H. Freeman; New York: 2008.

(60). Rees DC, Congreve M, Murray CW, Carr R. Fragment-based lead discovery. Nat. Rev. Drug Discovery. 2004; 3:660–672.

(61). Veber DF, Johnson SR, Cheng HY, Smith BR, Ward KW, Kopple KD. Molecular properties that influence the oral bioavailability of drug candidates. J. Med. Chem. 2002; 45:2615–2623. [PubMed: 12036371]

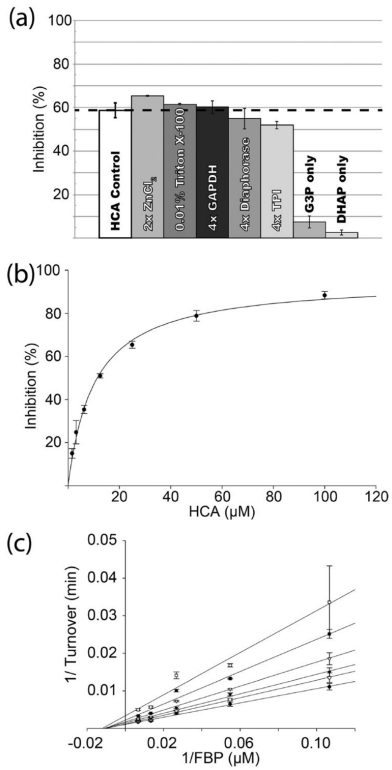

Figure 1.

Kinetic studies of HCA's inhibition of MtFBA. (a) HCA (25 μM) was tested for its ability to inhibit MtFBA activity in the presence of 50 μM $ZnCl_2$, 0.01% Triton X-100, and a 160-fold excess of coupling enzymes GAPDH, diaphorase, and MtTPI or FBP products G3P and DHAP (75 μM). The dashed line is drawn from the control of 25 μM HCA to aid in comparison. Error bars represent the standard deviation from the average. (b) Plot of HCA concentration in the presence of a 2-fold excess of $ZnCl_2$ as the HCA concentration was varied from 0 to 100 μM using the Michaelis–Menten equation to determine the IC_{50}. (c) Lineweaver–Burke plot of inhibition of MtFBA by HCA. Concentrations of HCA in the presence of a 2-fold excess of $ZnCl_2$ were (●) 0, (◯) 1.625, (▼) 3.125, (▽) 6.25, (■) 12.5, and (□) 25 μM. Data were globally fit to a pure noncompetitive inhibition model.

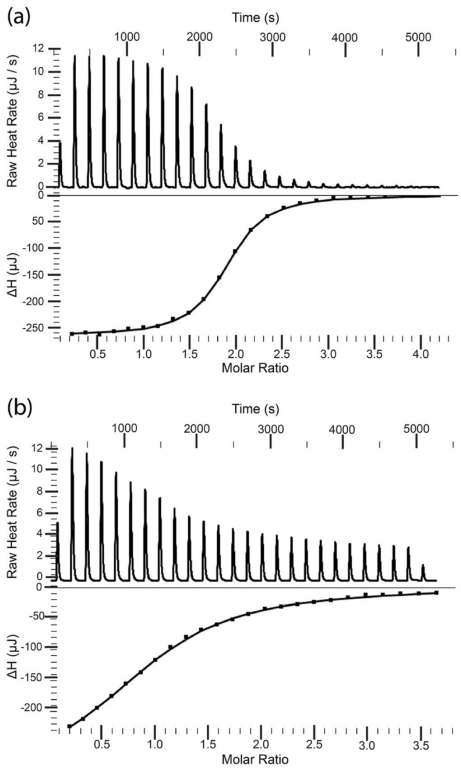

Figure 2.

ITC binding of MtFBA with HCA. The top panel represents the raw heat data from 25 injections at 25 °C, and the bottom panel shows the integrated heat peak areas plotted vs the molar ratio of (a) HCA to $ZnCl_2$ or (b) HCA in the presence of excess $ZnCl_2$ to MtFBA. The last five data points were averaged for the heat of dilution and subtracted from the rest of the data. The lines represent the best fits to an independent mode. This figure was generated using the NanoAnalyze software provided by TA Instruments.

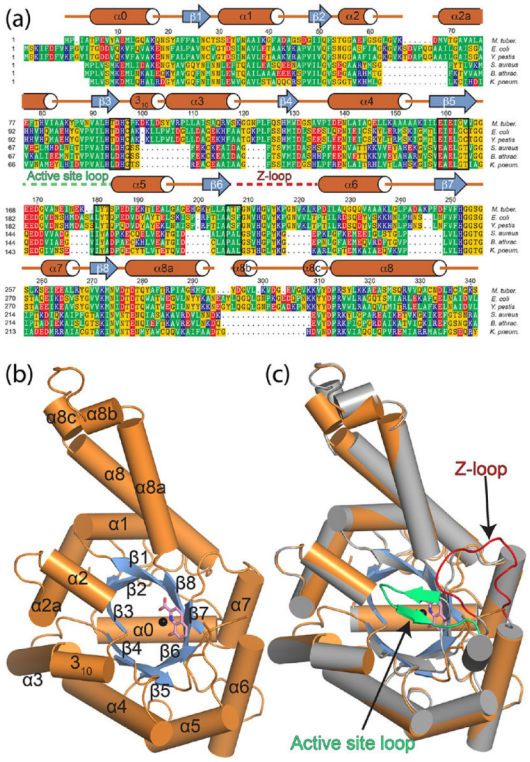

Figure 3.

Sequence alignment of class II FBAs and X-ray structure of MtFBA in complex with HCA. (a) FBAs are from *M. tuberculosis* (*M. tuber*; NP_334786), *E. coli* (*E. coli*; PDB entry 1B57_A), *Yersinia pestis* (*Y. pestis*; ZP_04518851), *S. aureus* (*S. aureus*; Q5HE75), *Bacillus anthracis* (*B. anthrac*; PDB entry 3Q94_A), and *Klebsiella pneumoniae* (*K. pneum*; ZP_14594173). The secondary structure of the MtFBA–HCA complex according to Defined Secondary Structure of Proteins (DSSP) is shown as orange cylinders (helical regions), blue arrows (β-sheets), and orange lines (loops). Dashed lines represent residues for which electron density was not defined in the crystal structure. Breaks denote regions where MtFBA does not have residues. Black brackets indicate residues that are part of MtFBA's active site. (b) Cartoon rendering of the MtFBA–HCA protomer. Helical regions are represented as cylinders and β-strands as arrows. Helices and loops are colored orange and β-strands blue; HCA is shown as pink sticks, and zinc ion is shown as a black sphere. (c) Same MtFBA–HCA complex shown in panel b but overlaid with the MtFBA–PGH complex (PDB entry 4DEL) colored gray. Residues 167–177 (green) and 210–223 (red) for which density is observed in the MtFBA–PGH structure but not in the MtFBA–HCA structure.

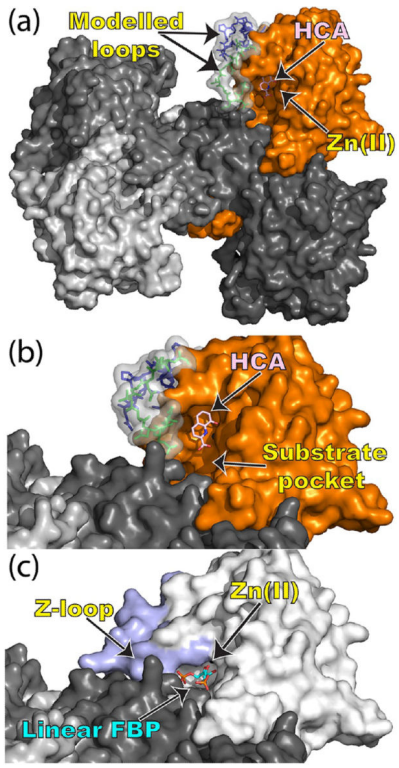

Figure 4.

Rearrangement of the substrate pocket caused by HCA binding. (a) Surface rendering of the MtFBA–HCA complex as its tetrameric biological assembly with one MtFBA protomer colored orange, the rest colored various shades of gray, and HCA rendered as pink sticks. Loops that were modeled in due to a lack of electron density are shown as transparent surfaces and either green sticks (residues 167–177) or blue sticks (residues 210–223). (b) Close-up of the substrate binding pocket of the MtFBA–HCA complex. (c) Close-up of the substrate binding pocket for MtFBA (white) bound with linear fructose 1,6-bisphosphate (cyan sticks; PDB entry 3ELF), in which residues 210–223 are colored light blue. In all cases, the zinc ions are rendered as a black sphere.

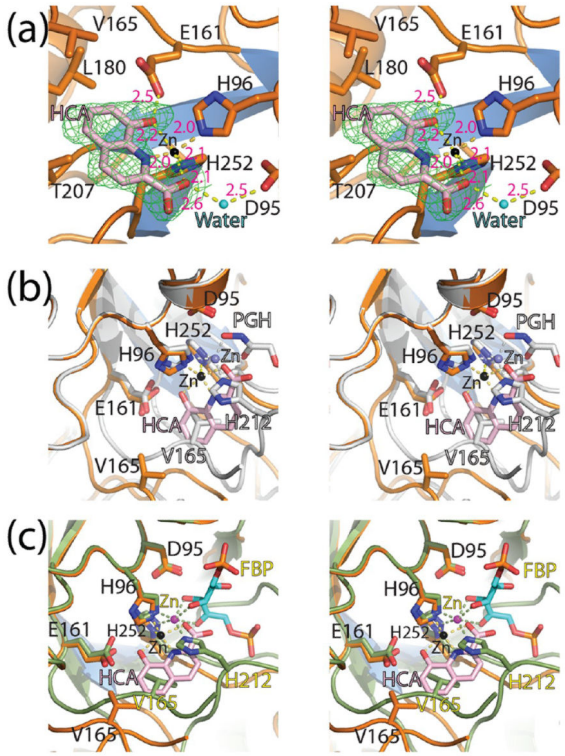

Figure 5.

Comparison of the active sites of class II FBAs. (a) Wall-eyed stereoview close-up of HCA interacting with MtFBA and zinc. Green mesh represents $F_o - F_c$ density scaled to 3σ; black labels indicate MtFBA residues, and hot pink labels and dashed lines indicate distances measured in angstroms. (b) Wall-eyed stereoview of MtFBA (orange) bound to HCA (pink) interacting with Zn (black) overlaid with MtFBA interacting with PGH (gray; PDB entry 4DEL) and Zn (purple), with dashed lines indicating bonding interactions. (c) Wall-eyed stereoview of MtFBA bound to HCA interacting with Zn colored as in panel b overlaid with MtFBA (green) interacting with FBP (cyan; PDB entry 3ELF) and Zn (magenta) with dashed lines indicating bonding interactions.

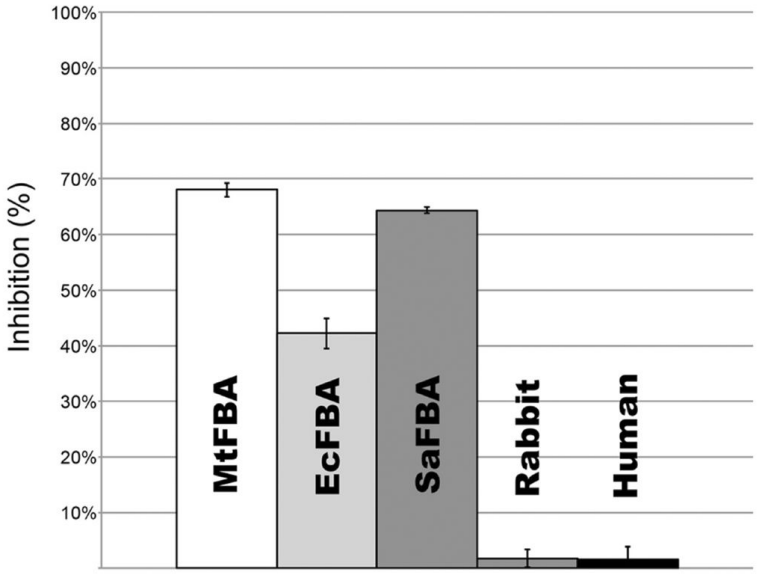

Figure 6.

Effectiveness of HCA against class I FBAs and other class II FBAs. HCA at 25 μM was tested for its ability to inhibit class II FBAs from *E. coli* and MRSA as well as class I FBAs isolated from either rabbit or human muscle. Error bars represent the standard deviations from the average.

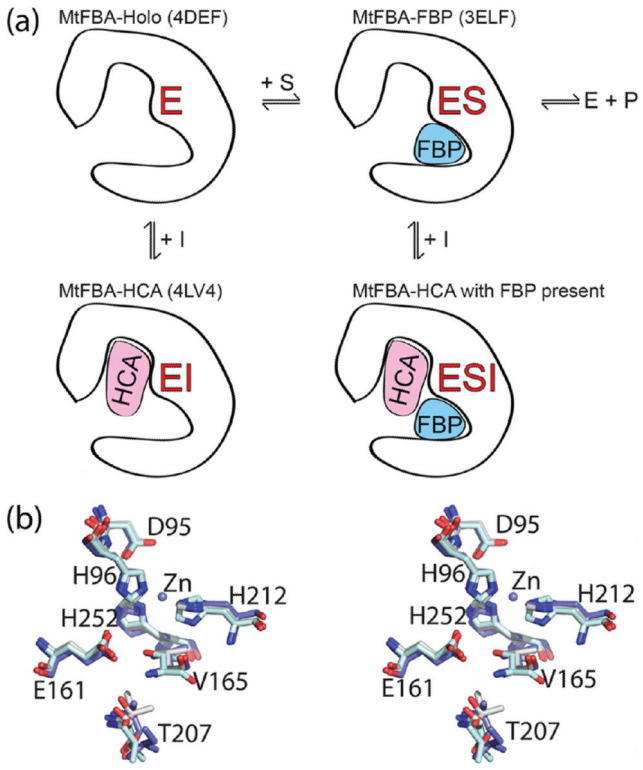

Figure 7.

Proposed model of inhibition of HCA for MtFBA and applicability to other class II FBAs. (a) Cartoon adaptation of HCA's inhibition of MtFBA according to the third model for noncompetitive inhibition. (b) Wall-eyed stereoview of the overlay of FBAs from *M. tuberculosis* (gray; PDB entry 4DEL), *B. anthracis* (blue; PDB entry 3Q94), and *E. coli* (teal; PDB entry 1B57). Black labels indicate MtFBA residues.

Table 1

Data Collection and Refinement Statistics for the MtFBA–HCA Complex

Data Collection	
space group	*I*222
unit cell dimensions	
a, *b*, *c* (Å)	60.6, 118.9, 165.2
α = β = γ (deg)	90
resolution (Å)	50.0–2.10
no. of reflections observed	145672
no. of unique reflections	36003
R_{merge} (%)[a]	9.9 (28.5)[c]
$I/\sigma I$	16.4 (3.5)[c]
completeness (%)	98.6 (87.0)[c]
Refinement	
resolution range (Å)	50–2.10
no. of reflections in the working set	35983
no. of reflections in the test set	1799
R_{work} (%)[b]	16.1 (17.3)[c]
R_{free} (%)[b]	19.1 (20.3)[c]
root-mean-square deviation	
bond lengths (Å)	0.01
bond angles (deg)	1.0
no. of protein/water/ligand atoms	2464/357/40
average *B* factor (Å^2)	
total	30.8
protein	28.9
water	41.2
ions	33.8
ligands	44.6
HCA	43.4

[a] $R_{merge} = \Sigma_h\Sigma_i|I_i(h) - \langle I(h)\rangle|/\Sigma_h\Sigma_i I_i(h)$, where $I_i(h)$ is the *i*th measurement and $\langle I(h)\rangle$ is the weighted mean of all measurements of $I(h)$.

[b] R_{work} and $R_{free} = h[|F(h)_{obs}| - |F(h)_{calc}|]/h|(h)_{obs}|$ for reflections in the working and test sets, respectively.

[c] Data for the last resolution shell are given in parentheses.